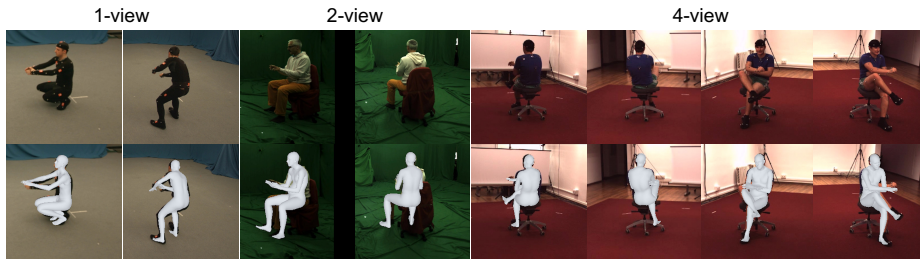


# Human Mesh Recovery from Arbitrary Multi-view Images

Xiaoben Li<sup>1,2</sup>, Mancheng Meng<sup>2</sup>, Ziyang Wu<sup>2</sup>, Terrence Chen<sup>2</sup>, Fan Yang<sup>2\*</sup>, and Dinggang Shen<sup>1,2</sup>

<sup>1</sup> ShanghaiTech University

<sup>2</sup> United Imaging Intelligence



**Fig. 1: Unified Human Mesh Recovery (U-HMR): Recovering human pose and shape from arbitrary multi-view images.** We propose a concise, flexible, and effective framework for human mesh recovery from arbitrary multi-view images. From left to right the results of human mesh recovery from 1-view, 2-view, and 4-view images (from three different datasets) are shown respectively. Our framework can be directly adapted to arbitrary number of views without any modification, fine-tuning or re-training, and can learn multi-view information effectively for human mesh recovery. For the limitation of page space, up to 4-view results are displayed here. Results on more views are in supplementary material.

**Abstract.** Human mesh recovery from arbitrary multi-view images involves two characteristics: the arbitrary camera poses and arbitrary number of camera views. Because of the variability, designing a unified framework to tackle this task is challenging. The challenges can be summarized as the dilemma of being able to simultaneously estimate arbitrary camera poses and recover human mesh from arbitrary multi-view images while maintaining flexibility. To solve this dilemma, we propose a divide and conquer framework for Unified Human Mesh Recovery (U-HMR) from arbitrary multi-view images. In particular, U-HMR consists of a decoupled structure and two main components: camera and body decoupling (CBD), camera pose estimation (CPE), and arbitrary view fusion (AVF). As camera poses and human body mesh are independent of each other,

\* Corresponding author.

CBD splits the estimation of them into two sub-tasks for two individual sub-networks (*i.e.*, CPE and AVF) to handle respectively, thus the two sub-tasks are disentangled. In CPE, since each camera pose is unrelated to the others, we adopt a shared MLP to process all views in a parallel way. In AVF, in order to fuse multi-view information and make the fusion operation independent of the number of views, we introduce a transformer decoder with a SMPL parameters query token to extract cross-view features for mesh recovery. To demonstrate the efficacy and flexibility of the proposed framework and effect of each component, we conduct extensive experiments on three public datasets: Human3.6M, MPI-INF-3DHP, and TotalCapture.

**Keywords:** Human mesh recovery · Arbitrary multi-view images · Divide and conquer

## 1 Introduction

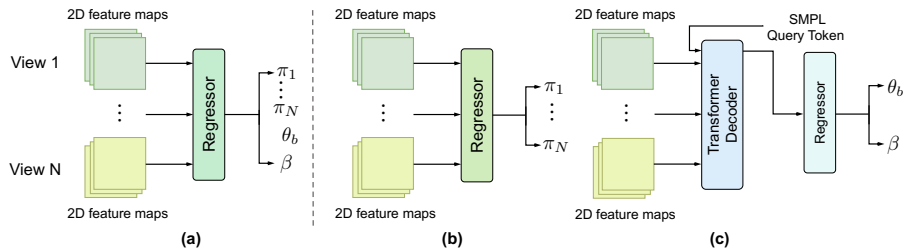


**Fig. 2: The comparison of multi-view scenario with a coupled structure (left) and arbitrary multi-view scenario with a decoupled structure (right).** (a): The conventional model structure for human mesh recovery from multi-view image. (b): The model structure of camera pose  $\pi_i$  estimation for arbitrary number of views, note that the regressor here is shared across different views. (c): The model structure of arbitrary multi-view feature fusion for body pose  $\theta_b$  and shape  $\beta$  estimation.

Human mesh recovery [1, 20, 45] as a fundamental task in computer vision involves estimating both the pose and shape of the human body and producing mesh representation of the human body from input visual data. It has a wide range of applications, including human-computer interaction, augmented reality, and virtual reality. Due to the critical importance and broad applications, numerous works have been conducted in this field.

Considerable amount of efforts are spent on recovering human mesh from a single image [1, 11, 20, 22, 24, 45]. Although those methods can recovery human mesh from any single-view image, it is an ill-posed task because of depth ambiguity and possible occlusion. As multi-view images inherently contain more

comprehensive information and multi-camera systems that can capture multi-view images are becoming more common, it is more feasible for human mesh recovery.

Considering that multi-view images contain crucial information for human mesh recovery, such as camera poses, human pose and shape from each view, and cross-view 3D geometry, many works [19, 31, 47, 61] have been conducted to explore the usability of the above information. However, most of them are restricted to scenarios with fixed camera poses or number of views. The structure of these methods can be summarized into Fig. 2 (a). While some methods can also be applied to arbitrary multi-view scenarios [19, 61], they focus on multi-view fusion and their model structures are complicatedly designed in order to effectively leverage the aforementioned multi-view information but not paying much attention to the flexibility. More importantly, to the best of our knowledge, no attempts have been made to systematically investigate how to design a concise and unified network architecture to efficiently and effectively accommodate arbitrarily varied camera poses and number of views for human mesh recovery.

We follow the HMR [11, 20] direction to recover human mesh. Designing a concise framework for arbitrary multi-view images is a challenging task, because the “arbitrary” contains two properties: 1) the poses of cameras are arbitrary, 2) the number of views is arbitrary. The arbitrary poses of cameras lead to the requirement of simultaneous camera pose estimation and mesh recovery, which increases the difficulty of model learning. Moreover, since both camera pose estimation and human mesh recovery from multi-view images are closely related to the number of views, this further rises the difficulty of dealing with arbitrary multi-view images with a single network.

We observe that the camera poses and human body mesh (pose and shape) are naturally uncorrelated to each other. In addition, each camera pose is independent of others, so that estimating one camera pose is actually identical to estimating arbitrary number of camera poses. Therefore, if we can separate camera pose estimation and human mesh recovery (Fig. 2 right), at least the camera pose estimation task can be relatively easy to achieve independence from number of views (Fig. 2 (b)).

In terms of the multi-view feature fusion for human mesh recovery, the flexibility of fusion network structure is constrained by the number of views. Inspired by the query based transformer decoder structure [2, 11, 35], the multi-view fusion can be modeled by using a query token to integrate feature from different locations and views for body pose and shape estimation (Fig. 2 (c)). In this way, the structure of fusion network is not influenced by the number of views.

Based on the analysis above, we propose a divide and conquer strategy to deal with the difficulties. Specifically, we construct a concise network architecture, named Unified Human Mesh Recovery network (U-HMR). The network is mainly composed by a camera and body decoupling structure (CBD), a camera pose estimation module (CPE), and an arbitrary view fusion module (AVF). CBD divides the human mesh recovery into two sub-tasks: camera pose estimation and body pose/shape estimation, for two independent sub-networks to

handle. Consequently, it can mitigate the model learning difficulty. In addition, 3D human pose and shape is independent of the camera pose, CBD is intuitively aligned with this observation. As the camera poses of different views are not correlated with each other, we adopt a weight-shared MLP in CPE to process camera poses in a parallel manner. To alleviate the dependency on number of views in multi-view fusion, we introduce a transformer decoder with a SMPL parameters query token in AVF, so that the cross-view image features can be aggregated regardless of the varying number of views. Furthermore, it also work well in a single view scenario because of its flexibility for arbitrary number of views.

Our contributions can be summarized as follows:

1. We comprehensively investigate how to design a concise and unified framework for human mesh recovery from arbitrary multi-view images, and propose a divide and conquer architecture by decoupling camera pose estimation and human mesh recovery.
2. We propose to introduce transformer decoder with a SMPL parameters query token to aggregate the multi-view feature.
3. We conduct extensive experiments on large datasets to validate the flexibility and efficacy of our method and proposed components.

## 2 Related Work

**Human Mesh Recovery for a Single Image.** Works in this field are roughly divided into two categories: optimization-based methods and regression-based methods. Optimization-based methods [1, 12, 13, 27, 44, 49, 52, 57, 62] usually fit a parametric human body model, *e.g.*, SMPL [37], to input image by iteratively minimizing the difference between the projected 3D mesh and the 2D observations, while regression-based methods [20, 22, 23, 25, 29, 39, 42, 45, 66, 68, 69] use deep neural networks to directly regress the 3D mesh from input image. In the scope of this paper we focus on regression-based methods. Starting from HMR [20], numerous methods have been proposed to improve the performance of human mesh recovery. Most of them investigate more comprehensive feature representation for the regression of SMPL parameters. However, the performance of the methods are still constrained due to the inherent depth ambiguity and possible occlusion of single image.

As transformer [55] has been successfully used in many computer vision applications [2, 6, 14], it is also used for human mesh recovery. METRO [33] and Graphormer [34] introduce transformer encoder to model global interactions among mesh vertices and joints. Following METRO, several methods are proposed to reduce computational cost [3, 7, 68, 69] or leverage pixel-aligned features [21, 60]. While METRO and its followers mostly focus on non-parametric mesh recovery, transformers can also be used in parametric mesh recovery. Yang *et al.* [59] propose a novel Transformer-based model with a design of independent tokens which are updated to estimate SMPL parameters conditioned on a given

image. OSX [32] proposes one-stage framework with component-aware transformer to capture the connections of body parts and output whole-body model parameters [44]. In 4DHumans [11], HMR2.0, a fully “transformerized” version of network for human mesh recovery, is proposed. HMR2.0 uses ViT [6] as the image encoder and a standard transformer decoder with multi-head self-attention to produce human model parameters. Our method benefits from advance of transformer as well by using a transformer decoder-based framework to fuse multi-view information. For a more comprehensive review, we refer readers to a survey on recovering 3D human mesh from monocular images [51].

**Human Mesh Recovery from Multi-view Images.** Multi-view images inherently contain more comprehensive information, making it more feasible for human mesh recovery [5, 19, 31, 47, 61]. Since more works focus on multi-view 3D human pose estimation (3DHPE) and can inspire multi-view human mesh recovery, we include some works on this topic here. When camera calibrations (intrinsic and extrinsic) are available, multi-view information can be integrated using multi-view geometry. In [5, 18, 47], 2D features from multi-view images are back-projected and aggregated into a 3D feature volume using camera calibrations. 3D geometry information can also be fused into 2D features [16, 38] using epipolar geometry for multi-view 3D human pose estimation. But camera calibration is not easy to obtain, especially in some dynamic scenes. When camera calibrations are unavailable, multi-view information is usually fused via learning based methods. In [48, 70], multi-view information is fused by Transformer for multi-view 3D human pose estimation without camera calibrations. As for human mesh recovery, Liang *et al.* [31] use a recurrent module to predict human model and camera parameters view by view and stage by stage. Yu *et al.* [61] leverage the human body as a semantic calibration target, in which way multi-view features are aligned and fused without the need of camera calibrations. Instead of focusing on multi-view information fusion, our work is to solve the entanglement of body mesh, camera pose, and arbitrary multi-view in estimating SMPL parameters.

### 3 Method

#### 3.1 Human Body Representation

The SMPL (Skinned Multi-Person Linear Model) model [37] is a skinned vertex-based model and can accurately represent a wide variety of body shapes in natural human poses. It provides a function  $M(\theta, \beta; \Phi) : \mathbb{R}^{|\theta| \times |\beta|} \mapsto \mathbb{R}^{3N}$ , mapping pose and shape parameters to  $N = 6,890$  vertices to form a mesh representation of human body. In the function  $\theta \in \mathbb{R}^{24 \times 3}$ ,  $\beta \in \mathbb{R}^{10}$ , and  $\Phi$  are pose, shape, and model parameters, respectively. The pose parameters  $\theta$  includes global rotation  $\theta_g \in \mathbb{R}^3$  which is unrelated to the body pose and body pose parameters  $\theta_b \in \mathbb{R}^{23 \times 3}$ , consequently  $\theta = \{\theta_g, \theta_b\}$ . The shape parameters  $\beta$  is coefficient of a low-dimensional shape space, learned from a training set of thousands of registered scans.

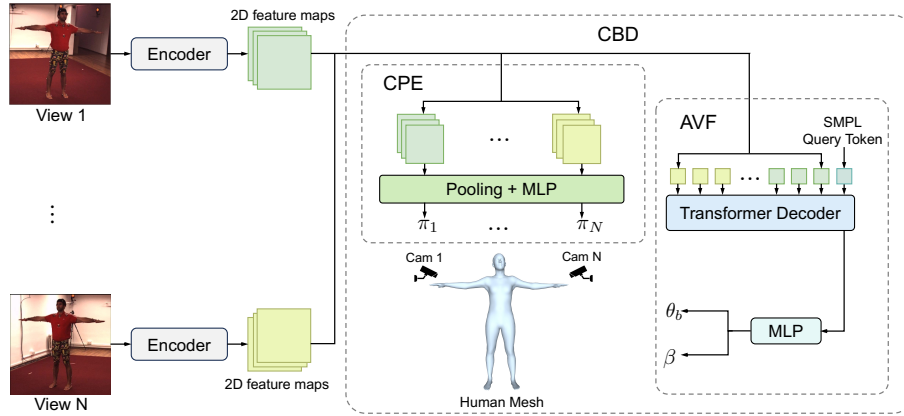


**Fig. 3: Overview of the proposed framework.** We divide the task of reconstructing 3D human mesh from arbitrary multi-view images into two sub-tasks: 1) the estimation of camera parameters, 2) the estimation of body mesh (pose & shape) parameters. This is achieved by a camera and body decoupling structure (CBD). Given  $N$  images of a human from different camera views, we first extract 2D features from each image using a 2D image encoder. Then the 2D feature maps are forwarded to two modules, camera pose estimation module (CPE), and arbitrary view fusion module (AVF). In CPE, feature maps of each view are fed into an MLP, which is shared across views, to predict camera parameters  $\pi_i$  of each view independently. In AVF, feature maps from all views are reshaped into tokens and forwarded into a transformer decoder. Inspired by PETR [35], multi-view position embeddings are adopted to distinguish the tokens of different regions and views. A single learnable SMPL query token is introduced to attend tokens from multi-view images to form a cross-attention structure, so that the multi-view information is implicitly encoded into the SMPL query token which is subsequently used to produce final body pose parameters  $\theta_b$  and shape parameters  $\beta$ .

Typically, a pre-trained linear regressor  $W$  is used to obtain  $k$  keypoints of interest of the whole body, *i.e.*,  $J_{3D} \in \mathbb{R}^{k \times 3} = WM(\theta, \beta; \Phi)$  [24]. As for 2D keypoints, a perspective camera model with fixed focal length and intrinsics  $K$  is used to project 3D joint positions into 2D image plane. Each camera pose  $\pi = \{R, t\}$  consists of a global orientation  $R \in \mathbb{R}^3$  and a translation  $t \in \mathbb{R}^3$ . Given above parameters, 3D keypoints can be projected to 2D image as  $J_{2D} = \Pi(K(RJ_{3D} + t))$ , where  $\Pi$  is a perspective projection with camera intrinsics  $K$ . Since the pose parameters  $\theta$  already includes a global orientation  $\theta_g$  which can represent the camera rotation, in practice we consider  $R = \theta_g$ , so when reconstructing human body from a single image, we estimate body pose parameters  $\theta_b$  and camera pose  $\pi = \{R, t\}$ , and when reconstructing human body from  $N$  images, we estimate body pose parameters  $\theta_b$  and  $N$  camera poses  $\pi_i = \{R_i, t_i\}_{i=1}^N$ .

### 3.2 Unified Human Mesh Recovery (U-HMR)

**Overview.** The overall architecture of proposed Unified Human Mesh Recovery network (U-HMR) is depicted in Fig. 3. Generally, U-HMR is composed by 1. a 2D image encoder, 2. a camera and body decoupling structure (CBD), 3. a camera pose estimation module (CPE), and 4. an arbitrary view fusion module (AVF). Given images of a human body from  $N$  camera views, we first extract 2D features  $f_i$  from each image  $I_i$  using a shared 2D image encoder  $E$ , where  $f_i = E(I_i)$ . The instantiation of the encoder can be any visual fundamental model (*e.g.*, ResNet, ViT). These features are simultaneously forwarded into CPE and AVF modules via a bifurcating operation in CBD. CPE predicts all camera poses  $(\pi_i, \dots, \pi_N)$  with a view-invariant MLP network. AVF integrates cross-view features with a transformer decoder by introducing a SMPL query token which attends tokens from multi-view images and is forwarded into an MLP to output human body pose  $\theta_b$  and shape  $\beta$ . Note that even in single view scenario, the proposed framework can work well.

**Camera and Body Decoupling (CBD).** The 3D human body pose and shape are independent of camera poses. Therefore, it is natural and intuitively reasonable to divide the camera pose estimation and human mesh recovery to two individual sub-tasks. Moreover, in arbitrary multi-view scenario, both camera pose estimation and human mesh recovery are heavily related with the number of camera views. This entanglement results in the rising difficulty of dealing with arbitrary number of views. By decoupling the two tasks, we can handle the arbitrary problem in a divide-and-conquer manner and make it easier to eliminate the dependence of sub-tasks on the number of camera views.

**Camera Pose Estimation (CPE).** While the computation complexity of estimating camera pose is linearly correlated with the number of views, the camera pose of each view is independent of others. Consequently, the model complexity can be detached from the number of views. Specifically, we adopt a cross-view shared MLP network to predict all camera poses in a parallel way. In this way, the network structure of estimating camera pose is completely disentangled with the number of views, so as to adapt to arbitrary multi-view scenario. The formally expression of the whole CPE module is:

$$\{\pi_i\}_{i=1}^N = \{F_c(f_i)\}_{i=1}^N \quad (1)$$

where  $f_i$ ,  $\pi_i$ , and  $F_c$  denote the image feature, camera pose, and MLP, and  $N$  is the number of views.

**Arbitrary View Fusion (AVF).** In terms of fusing arbitrary multi-view features for human mesh recovery, we expect the following two properties: 1) the complementary information from different views should be effectively fused, 2) the fusion operation should be unrelated with the number of views. To achieve these properties, we introduce a transformer decoder-based architecture with a query token to aggregate cross-view features. Specifically, given 2D features  $\{f_i\}_{i=1}^N$  from all views, we first reshape them into tokens and feed them into a transformer decoder  $\Omega$ . Inspired by PETR [35], multi-view position embeddings are added to the tokens to distinguish tokens from different regions and views.

Furthermore, to fuse the information of different regions and views, we introduce a single learnable SMPL query token,  $q$ , to attend tokens from multi-view images. After the cross-attention layers in the transformer decoder, the updated SMPL query token  $\hat{q}$  is expected to encode the information from tokens of multi-view images. Then a light-weight MLP,  $F_b$ , predicts the pose parameters  $\theta_b$  and shape parameters  $\beta$  from the updated SMPL query token  $\hat{q}$ . The computation process from the 2D features to the predicted parameters can be expressed as follows:

$$\begin{aligned} \hat{q} &= \Omega(q, \{f_i + p_i\}_{i=1}^N) \\ \{\theta_b, \beta\} &= F_b(\hat{q}) \end{aligned} \quad (2)$$

Essentially, the multi-view feature fusion is a process of weighted sum of each view feature. In the transformer decoder structure, because of the cross-attention mechanism, the number of the weights is not hard coded in network, it is varying with the number of tokens. Due to this online variability, we can fuse features from arbitrary multi-view images. In addition, benefiting from the feature representation learning ability of the transformer decoder, the the updated SMPL query token can be more representative for human mesh recovery.

### 3.3 Loss Functions

Following the best practice of the HMR [20] and HMR2.0 [11], we use a combination of 2D reprojection losses, 3D losses including 3D keypoints losses and SMPL parameters losses, and adversarial losses provided by a discriminator. During the training process, they are empirically weighted. The loss functions are slightly different in multi-view setting. When the ground-truth SMPL pose parameters  $\hat{\theta}$  and shape parameters  $\hat{\beta}$  are available, we supervise the model predictions using a squared L2 loss:

$$\mathcal{L}_{smpl} = \|\theta - \hat{\theta}\|_2^2 + \|\beta - \hat{\beta}\|_2^2.$$

When accurate ground-truth 3D keypoints  $\hat{J}_{3D}$  are available in the dataset, a L1 loss is adopted to measure the difference of predicted 3D keypoints  $J_{3D}$  with  $\hat{J}_{3D}$ . Since camera parameters for each view are estimated, we can use them to transform 3D keypoints from SMPL coordinate system to the coordinate system of each camera, *i.e.*, our predicted 3D keypoints  $J_{3D}$  are in the camera coordinate system. The total loss is the sum of losses from all views:

$$\mathcal{L}_{3D} = \sum_i^N \|J_{3D}^i - \hat{J}_{3D}^i\|_1.$$

When the dataset provides accurate 2D keypoints annotations  $\hat{J}_{2D}$ , we supervise the model training with a L1 loss of the 2D projection of predicted 3D keypoints  $J_{2D}$  with respect to  $\hat{J}_{2D}$ . 2D reprojection loss is often considered to encourage pixel-level alignment. Similar to the 3D loss, the total 2D loss is the sum of losses from all views:

$$\mathcal{L}_{2D} = \sum_i^N \|J_{2D}^i - \hat{J}_{2D}^i\|_1.$$



In addition, we want to ensure that our model predicts valid 3D poses and use the adversarial prior proposed in HMR [20] to regularize the prediction. It factorizes the model parameters into: (i) body pose parameters  $\theta_b$ , (ii) shape parameters  $\beta$ , and (iii) per-part relative rotations  $\theta_i$ , which is one 3D rotation for each of the 23 joints of the SMPL model. A discriminator  $D_k$  is trained for each factor of the body model, where  $k$  denotes the index of factors. The generator loss can be expressed as following:

$$\mathcal{L}_{adv} = \sum_k (D_k(\theta_b, \beta) - 1)^2.$$

## 4 Experiments

### 4.1 Experimental Setup

**Datasets.** We evaluate our method on three large multi-view motion capture datasets, *i.e.*, Human3.6M [17], MPI-INF-3DHP [41], and TotalCapture [53]. Particularly, on Human3.6M we comprehensively investigate how to design a framework for human mesh recovery from arbitrary multi-view images and conduct extensive experiments to validate the effect of proposed components. To demonstrate the superiority of the proposed method, the comparison with state-of-the-art (SOTA) methods is performed on all three datasets.

Human3.6M is a large 3D human pose benchmark, containing 11 different subjects and each subject with 15 different daily indoor actions. The subjects are captured by 4 synchronized 50 Hz digital cameras. The dataset provides 2D/3D keypoint annotations obtained by marker-based motion capture system. The SMPL annotations are obtained by applying MoSh [36] to the sparse 3D MoCap marker following previous works [20, 25]. Similar to [20, 31, 47], we follow the protocol 1 to use subjects 1, 5, 6, 7, and 8 for training and subjects 9 and 11 are for testing.

MPI-INF-3DHP contains 8 actors (4 males and 4 females) performing 8 human activities. 2D and 3D keypoint annotations are also provided by marker-less motion capture system. The dataset contains multi-view images of 14 cameras with regular lenses, and we choose views 0, 2, 7, 8 from them. Following [31, 47], the standard test dataset of MPI-INF-3DHP simply includes single-view images, we use subjects 1-7 for training and subject 8 for testing.

TotalCapture dataset consists of 1.9 million frames captured from 8 calibrated full HD video cameras recording at 60Hz. As suggested in [53], the training set consists of “ROM1,2,3”, “Walking1,3”, “Freestyle1,2”, “Acting1,2”, “Running1” on subjects 1, 2, and 3. The testing set consists of “Freestyle3”, “Walking2” and “Acting3” on subjects 1, 2, 3, 4, and 5. We use the images from four cameras (1, 3, 5, 7) in our experiments and do not use the IMU sensors.

**Evaluation Metrics.** For Human3.6M dataset, we use mean per joint position error (MPJPE) and reconstruction error as metrics. Reconstruction error is MPJPE after rigid alignment of the prediction with ground truth via Procrustes. The reconstruction error is also known as PA (procrustes aligned)-MPJPE. For

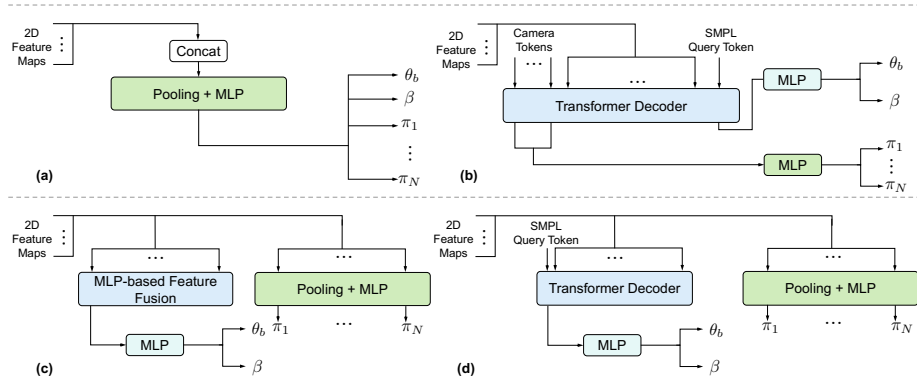


**Fig. 4: Different architecture designs for human mesh recovery from multi-view images.** The 2D feature maps are produced by the same 2D image encoder. All these variants output human mesh parameters and camera parameters of all views.

MPI-INF-3DHP, as this dataset is collected indoors and outdoors with a multi-camera marker-less MoCap system, thus the 3D annotations are less accurate. So in addition to MPJPE and PA-MPJPE, the Percentage of Correct Keypoints (PCK) thresholded at 150 mm and the Area Under the Curve (AUC) over a range of PCK thresholds with interval of 5 mm before and after rigid alignment are both reported on this dataset. For TotalCapture dataset, we report MPJPE and PA-MPJPE across different subjects and activity sequences.

**Implementation Details.** In our implementation, input size of all images is  $256 \times 256$ . For the 2D image encoder, we use the ResNet-50 [15] as the standard backbone following [20, 26, 30]. However, as depicted in [11], using a ViT backbone [6] achieves a significant improvement across the 3D and 2D metrics. Thus, in addition to ResNet-50, we also conduct experiments using a ViT backbone. As we use a combination of multiple losses, during training, we weight the different loss terms empirically as [11]. The model is trained for 100 epochs on 2 NVIDIA A100 GPUs and we use the AdamW optimizer with a learning rate of  $1e - 5$ ,  $\beta_1 = 0.9$ ,  $\beta_2 = 0.999$ , and a weight decay of  $1e - 4$ .

## 4.2 Ablation Studies

**Design of Decoupling and Multi-view Fusion.** We systematically investigate how to design a concise and unified network architecture to efficiently and effectively accommodate randomly varied camera poses and number of views. We design four different architectures for human mesh recovery from multi-view images, as shown in Fig. 4, we compare them both theoretically and empirically. (a) This is a simple extension of single-view HMR [20]. The 2D feature maps from different-view images are concatenated and pooled along two spatial dimensions (width and height), producing a single feature vector whose dimension is dependent on the number of views. Then the feature vector is forwarded to

**Table 1: Ablation study of different architecture designs.** To show the effect of different variants as much as possible, we use the powerful ViT as the 2D image encoder for all variants and report MPJPE and PA-MPJPE on Human3.6M dataset.

Variant	MPJPE ↓	PA-MPJPE ↓
(a) MLP	31.4	25.3
(b) Independent tokens	29.8	23.2
(c) Decoupling with MLP	36.9	25.3
(d) Decoupling with Transformer decoder	31.0	22.8

the MLP to output all parameters, including pose/shape parameters and camera parameters of all views. This architecture is concise but not flexible as the dimension of feature vector, *i.e.*, the dimension of the layers in the MLP, is dependent on the number of views. Moreover, the output dimension of the MLP is related with the number of camera pose as well, since this architecture produces the parameters all together. Thus it cannot be directly adapted to different number of camera views. **(b)** This architecture decouples camera parameters and body parameters to some extent. Camera parameters of different views and body parameters are represented as independent query tokens, which are used to produce corresponding parameters after processing in the transformer decoder. Although the estimation of body parameters is independent on the number of views, the number of camera query tokens still depend on the number of views, making this architecture unable to cope with an arbitrary number of views. **(c)** This architecture is similar to our final method while using an MLP for feature fusion instead of a transformer decoder. Given 2D feature maps of different views, unlike **(a)**, where the concatenating and pooling are employed to produce feature vector, we use an extra MLP to produce attention scores, *i.e.*, weights for different views, then the attention scores are normalized and used to calculate the weighted sum of features of different views to produce a fused feature vector, this fusion method is similar to the fusion of global features in [61]. This method is independent on the number of views, and has the same flexibility as our final method but with less feature representation capacity. **(d)** Our final method decouples the estimation of pose/shape and camera parameters, and uses a transformer decoder to fuse features from multi-view images.

The results of different architecture designs are presented in Tab. 1. We use the same 2D image encoder (*i.e.*, ViT) for the fair of comparison. Compared to other designs, our final method achieves best PA-MPJPE and second best MPJPE, and are adaptive to arbitrary multi-view scenario, which demonstrates the superiority of our method. In contrast to methods directly estimating parameters using MLP **(a)**, and fusing features from multi-view images using MLP **(c)**, our method outperforms them notably. It is worth noting that the performance of **(b)** is competitive to our final method **(d)**, and we consider this result can be attributed to three perspectives. First, both of these two designs adopt transformer decoder to aggregate features from multi-view images and achieve top-two results on both PA-MPJPE and MPJPE, demonstrating the powerful

**Table 2: Ablation study of number of views on Human3.6M dataset.** Note that PaFF [19] uses camera calibrations for fusion, and the results reported here are from the models re-trained using 2 and 3 views respectively, while Yu *et al.* [61] and our method require neither camera calibrations nor retraining, so the results of PaFF are expected to provide the performance upper bound. We use ResNet-50 as the 2D image encoder for our method as the other two methods do for the fair of comparison.

Method	Metrics	Number of views			
		4	3	2	1
PaFF [19]	MPJPE ↓	33.0	33.5	33.8	-
	PA-MPJPE ↓	26.9	27.5	27.6	-
Yu <i>et al.</i> [61]	MPJPE ↓	-	-	-	-
	PA-MPJPE ↓	33.0	34.2	37.3	44.1
Ours	MPJPE ↓	36.3	38.7	42.5	52.9
	PA-MPJPE ↓	28.3	30.9	34.5	42.5

capability of the transformer decoder for features fusion from multi-view images. Second, compared to PA-MPJPE, MPJPE indicates the error before rigid alignment, thus is able to demonstrate the accuracy of camera parameters estimation to some extent. In **(b)** the camera tokens also pass through the transformer decoder to produce camera parameters while in **(d)** the camera parameters are simply produced by the MLP from corresponding features. The intuitive reason is that the former method uses stronger features to predict camera parameters, thus has slightly lower MPJPE. Third, although **(b)** reports slightly lower MPJPE, it is less flexible than our final method. In other words, by a small compromise of the performance indicated by MPJPE, our final method provides a higher degree of flexibility, so that our method achieves better trade-off between performance and flexibility.

**Number of Views.** As we claim that our method can reconstruct human pose and shape for arbitrary multi-view images, to validate the flexibility, *i.e.*, the ability to adapt to different number of views, we conduct ablation study on the effect of varying number of views during inference phase. Since there have been two methods, Yu *et al.* [61] and PaFF [19], state that they can be applied to arbitrary number of views, we compare with them on Human 3.6M dataset and the results are shown in Tab. 2. For fair comparison, our model is trained with a combination of varying number of multi-view image (1-view, 2-view, 3-view, and 4-view), which is same as [61] does. While PaFF claims to have the ability to be applied to different number of views, the reported results are from the model retrained and tested using same number of views. Moreover, PaFF requires camera calibrations for feature fusion. So the results of PaFF can be expected to provide the performance upper bound of other two methods which are calibration-free and not retrained. Compared with Yu *et al.* [61], our method achieves better performance at any number of views.

**Table 3: Comparison results on Table 4: Comparison results on MPI-Human3.6M dataset.** We compare INF-3DHP dataset. The methods are our method with single-view, calibration- categorized from top to bottom as single-requiring multi-view, and calibration-free view, calibration-requiring multi-view, and multi-view methods. † denotes the output calibration-free multi-view methods of methods are non-parametric.

Method	Multi-view	Calibration-free	MPJPE ↓	PA-MPJPE ↓
SMPLiify [1]	No	-	-	82.3
Pavlakos <i>et al.</i> [45]	No	-	-	75.9
HMR [20]	No	-	88.0	56.8
NBF [43]	No	-	-	59.9
GraphCMR [25]†	No	-	-	50.1
HoloPose [13]	No	-	60.3	46.5
DenseRac [58]	No	-	76.8	48.0
SPIN [24]	No	-	62.5	41.1
DaNet [64]	No	-	61.5	48.6
DecoMR [63]†	No	-	-	39.3
LearnedGD [50]	No	-	-	56.4
Pose2Mesh [4]†	No	-	64.9	47.0
HKMR [9]	No	-	59.6	43.2
I2L-MeshNet [42]†	No	-	55.7	41.1
HybriK [28]	No	-	33.6	55.4
METRO [33]†	No	-	54.0	36.7
ProHMR [26]	No	-	-	41.2
Graphormer [33]†	No	-	51.2	34.5
PyMAF [66]	No	-	57.7	40.5
PARE [22]	No	-	76.8	50.6
CLIFF [29]	No	-	47.1	32.7
FastMETRO [3]†	No	-	52.2	33.7
PyMAF-X [65]	No	-	54.2	37.2
POTTER [68]	No	-	56.5	35.1
FeatER [69]	No	-	49.9	32.8
ProPose [8]	No	-	45.7	29.1
PLIKS [46]	No	-	47.0	34.5
PointHMR [21]†	No	-	48.3	32.9
VirtualMarker [39]	No	-	47.3	32.0
HMR 2.0a [11]	No	-	44.8	33.6
HMR 2.0b [11]	No	-	50.0	32.4
Yu <i>et al.</i> [61]	No	-	-	44.1
Ours (SV, ResNet-50)	No	-	52.9	42.5
Ours (SV, ViT)	No	-	43.3	32.6
MV-SPIN [47]	Yes	No	49.8	35.4
LVS [47]	Yes	No	46.9	32.5
PaFF [19]	Yes	No	33.0	26.9
LMT [5]	Yes	No	30.1	-
Liang <i>et al.</i> [31]	Yes	Yes	79.9	45.1
ProHMR [26]	Yes	Yes	62.2	34.5
Yu <i>et al.</i> [61]	Yes	Yes	-	33.0
Calib-free PaFF [19]	Yes	Yes	44.8	28.2
Ours (ResNet-50)	Yes	Yes	36.3	28.3
Ours (ViT)	Yes	Yes	31.0	22.8

Method	Absolute			Rigid Alignment		
	PCK ↑	AUC ↑	MPJPE ↓	PCK ↑	AUC ↑	MPJPE ↓
HMR [20]	72.9	36.5	124.2	86.3	47.8	89.8
SPIN [24]	76.4	37.1	105.2	92.5	55.6	67.5
ProHMR [26]	-	-	-	-	-	65.0
Ours (SV, ResNet-50)	71.3	24.3	77.8	94.3	50.0	64.5
Ours (SV, ViT)	99.2	66.1	54.5	99.3	73.3	43.7
LVS [47]	-	-	-	97.4	65.5	50.2
PaFF [19]	-	-	-	98.6	67.3	48.4
LMT [5]	-	-	-	96.6	71.6	45.9
Liang <i>et al.</i> [31]	72.0	35.0	126.0	95.0	65.0	59.0
Ours (ResNet-50)	94.0	44.0	55.4	98.8	71.0	39.8
Ours (ViT)	99.4	74.0	39.7	99.9	81.8	29.2

**Table 5: Comparison results on TotalCapture dataset.** We distinguish different methods by the input information from different sensors (Cameras and /or IMUs) provided by the dataset they use.

Method	Sensors	MPJPE ↓	PA-MPJPE ↓
VIP [40]	SV+IMUs	-	26.0
Kalman Filter [8]	SV+IMUs	34.7	23.1
ProPose [8]	SV+IMUs	28.5	21.2
ProPose [8]	SV	42.1	29.0
Ours (ResNet-50)	SV	41.4	28.9
Ours (ViT)	SV	38.5	27.2
PVH [53]	MV	107.3	-
Tri-CPM [56]	MV	99.8	-
IMUPVH [10]	MV+IMUs	42.6	-
GeoFuse [67]	MV+IMUs	24.6	20.6
ProPose [8]	MV+IMUs	23.5	19.4
ProHMR [26]	MV	127.8	-
Trumble <i>et al.</i> [54]	MV	85.4	-
Ours (ResNet-50)	MV	36.4	26.1
Ours (ViT)	MV	29.2	21.2

### 4.3 Comparison with State-of-the-art Methods

**Human3.6M.** The comparison results on Human3.6M dataset are shown in Tab. 3. As our method is suitable for arbitrary multi-view images including single-view image, we also report the results of our method for single-view human body reconstruction as Yu *et al.* [61] do, which provides a fair comparison with other single-view methods. We report the results of method using ResNet-50 and ViT as 2D image encoder. For single-view human body reconstruction, our method achieves comparable results to latest SOTA method, *i.e.*, HMR 2.0, and achieves better results than Yu *et al.* [61]. As a calibration-free multi-view method, our method also achieves SOTA results which are comparable to, or even better than calibration-requiring methods.

**MPI-INF-3DHP.** The comparison results on MPI-INF-3DHP dataset are listed in Tab. 4. As the dataset is collected using marker-less MoCap system, the ground truth 3D annotations have some noise and is less accurate, thus PCK and AUC

**Table 6: Computational overhead** Efficiency analysis of the method using different number of views.

Number of Views	Parameters (M)		MACs (G)		Time (ms)	
	Backbone	Head	Backbone	Head	Backbone	Head
1			121.0	4.7	55.2	10.1
2			242.1	9.4	107.9	12.6
3	630.7	60.1	363.1	14.1	148.8	12.7
4			484.2	18.8	181.1	13.9

**Table 7: Sensitivity to input.** We perturb the centers and scales of ground truth bboxes in Human3.6M dataset and test model without retraining.

Method	ResNet-50		ViT	
	MPJPE	PA-MPJPE	MPJPE	PA-MPJPE
Ours	36.3	28.3	31.0	22.8
Ours (Perturbed)	59.5	39.4	46.8	30.1

are reported in addition to MPJPE, the results before and after rigid alignment are reported. We compare our method with single-view methods, calibration-requiring multi-view methods, and calibration-free multi-view methods. For reconstructing human body from multi-view images, our method outperforms both calibration-requiring and calibration-free methods. And our results of single-view reconstruction are also superior to the results from other single-view methods.

**TotalCapture.** Table 5 displays the comparison results on TotalCapture dataset. In addition to RGB cameras, the dataset also provides information from IMU sensors and some methods use the information as the input. So we distinguish different methods by the input information from different sensors (cameras and /or IMUs) provided by the dataset they use.

#### 4.4 Computational Overhead

To validate the efficiency, we analyze the computational overhead of our method. We report the number of parameters, multiply-add operations (MACs), and time consumption per sample of different number of views in Tab. 6. For clearer illustration, we divide the whole model into two parts, the backbone (ViT), for feature extraction and the head (both CPE and AVF) for camera and human body mesh parameters estimation. The results show that the head adds very little parameters and computational overhead compared to the ViT backbone, which means that our method is efficient.

#### 4.5 Sensitivity to Input

Although we use ground-truth bounding boxes of human in our experiments, in real applications, there would be imperfect detection/crop such as scale changes and center shifts. To investigate the effect of inaccurate detection/crop, we perturb the input images from Human3.6M, *i.e.*, add random center shifts ( $\pm 20$  pixels) and randomly change the scales (0.8-1.2), then test using the perturbed images without retraining, the results are in Tab. 7. We observe that imperfect crop does affect performance, but the performance degradation is acceptable, especially with ViT as backbone. On one hand, ViT is stronger and produces more robust features, and on the other hand, our method could fuse information from different views effectively thus the imperfections of the crops could be suppressed.

## 5 Conclusion

We propose a simple, flexible, and effective framework using a divide and conquer strategy for human mesh recovery from arbitrary multi-view images. Based on the observation that camera poses and human mesh are independent of each other, we split the estimation of them into two sub-tasks. For the estimation of camera poses, we use a single shared MLP to process all views in a parallel way. For the estimation of human mesh, to fuse multi-view information effectively and make the fusion independent of the number of views, we introduce a transformer decoder with a SMPL query token to extract cross-view features for mesh recovery. The framework is not only adaptive to arbitrary multi-view images but also considerable effective in multi-view information fusion.

## References

1. [Bogo, F., Kanazawa, A., Lassner, C., Gehler, P., Romero, J., Black, M.J.: Keep it SMPL: Automatic estimation of 3D human pose and shape from a single image. In: ECCV \(2016\) 2, 4, 13](#)
2. [Carion, N., Massa, F., Synnaeve, G., Usunier, N., Kirillov, A., Zagoruyko, S.: End-to-end object detection with transformers. In: ECCV \(2020\) 3, 4](#)
3. [Cho, J., Youwang, K., Oh, T.H.: Cross-attention of disentangled modalities for 3d human mesh recovery with transformers. In: ECCV \(2022\) 4, 13](#)
4. [Choi, H., Moon, G., Lee, K.M.: Pose2Mesh: Graph convolutional network for 3D human pose and mesh recovery from a 2D human pose. In: ECCV \(2020\) 13](#)
5. [Chun, S., Park, S., Chang, J.Y.: Learnable human mesh triangulation for 3d human pose and shape estimation. In: WACV \(2023\) 5, 13](#)
6. [Dosovitskiy, A., Beyer, L., Kolesnikov, A., Weissenborn, D., Zhai, X., Unterthiner, T., Dehghani, M., Minderer, M., Heigold, G., Gelly, S., et al.: An image is worth 16x16 words: Transformers for image recognition at scale. In: ICLR \(2021\) 4, 5, 10](#)
7. [Dou, Z., Wu, Q., Lin, C., Cao, Z., Wu, Q., Wan, W., Komura, T., Wang, W.: Tore: Token reduction for efficient human mesh recovery with transformer. In: ICCV \(2023\) 4](#)
8. [Fang, Q., Chen, K., Fan, Y., Shuai, Q., Li, J., Zhang, W.: Learning analytical posterior probability for human mesh recovery. In: CVPR \(2023\) 13](#)
9. [Georgakis, G., Li, R., Karanam, S., Chen, T., Košecká, J., Wu, Z.: Hierarchical kinematic human mesh recovery. In: ECCV \(2020\) 13](#)
10. [Gilbert, A., Trumble, M., Malleson, C., Hilton, A., Collomosse, J.: Fusing visual and inertial sensors with semantics for 3d human pose estimation. IJCV \(2019\) 13](#)
11. [Goel, S., Pavlakos, G., Rajasegaran, J., Kanazawa, A., Malik, J.: Humans in 4D: Reconstructing and tracking humans with transformers. In: ICCV \(2023\) 2, 3, 5, 8, 10, 13](#)
12. [Guan, P., Weiss, A., Balan, A.O., Black, M.J.: Estimating human shape and pose from a single image. In: ICCV \(2009\) 4](#)
13. [Güler, R.A., Kokkinos, I.: HoloPose: Holistic 3D human reconstruction in-the-wild. In: CVPR \(2019\) 4, 13](#)
14. [He, K., Chen, X., Xie, S., Li, Y., Dollár, P., Girshick, R.: Masked autoencoders are scalable vision learners. In: CVPR \(2022\) 4](#)
15. [He, K., Zhang, X., Ren, S., Sun, J.: Deep residual learning for image recognition. In: CVPR \(2016\) 10](#)

16. He, Y., Yan, R., Fragkiadaki, K., Yu, S.I.: Epipolar transformers. In: CVPR (2020) [5](#)
17. Ionescu, C., Papava, D., Olaru, V., Sminchisescu, C.: Human3.6M: Large scale datasets and predictive methods for 3D human sensing in natural environments. IEEE TPAMI (2014) [9](#)
18. Isakov, K., Burkov, E., Lempitsky, V., Malkov, Y.: Learnable triangulation of human pose. In: ICCV (2019) [5](#)
19. Jia, K., Zhang, H., An, L., Liu, Y.: Delving deep into pixel alignment feature for accurate multi-view human mesh recovery. In: AAAI (2023) [3](#), [5](#), [12](#), [13](#)
20. Kanazawa, A., Black, M.J., Jacobs, D.W., Malik, J.: End-to-end recovery of human shape and pose. In: CVPR (2018) [2](#), [3](#), [4](#), [8](#), [9](#), [10](#), [13](#)
21. Kim, J., Gwon, M.G., Park, H., Kwon, H., Um, G.M., Kim, W.: Sampling is matter: Point-guided 3D human mesh reconstruction. In: CVPR (2023) [4](#), [13](#)
22. Kocabas, M., Huang, C.H.P., Hilliges, O., Black, M.J.: Pare: Part attention regressor for 3d human body estimation. In: ICCV (2021) [2](#), [4](#), [13](#)
23. Kocabas, M., Huang, C.H.P., Tesch, J., Müller, L., Hilliges, O., Black, M.J.: Spec: Seeing people in the wild with an estimated camera. In: ICCV (2021) [4](#)
24. Kolotouros, N., Pavlakos, G., Black, M.J., Daniilidis, K.: Learning to reconstruct 3d human pose and shape via model-fitting in the loop. In: ICCV (2019) [2](#), [6](#), [13](#)
25. Kolotouros, N., Pavlakos, G., Daniilidis, K.: Convolutional mesh regression for single-image human shape reconstruction. In: CVPR (2019) [4](#), [9](#), [13](#)
26. Kolotouros, N., Pavlakos, G., Jayaraman, D., Daniilidis, K.: Probabilistic modeling for human mesh recovery. In: ICCV (2021) [10](#), [13](#)
27. Lassner, C., Romero, J., Kiefel, M., Bogo, F., Black, M.J., Gehler, P.V.: Unite the people: Closing the loop between 3D and 2D human representations. In: CVPR (2017) [4](#)
28. Li, J., Xu, C., Chen, Z., Bian, S., Yang, L., Lu, C.: HybriK: A hybrid analytical-neural inverse kinematics solution for 3D human pose and shape estimation. In: CVPR (2021) [13](#)
29. Li, Z., Liu, J., Zhang, Z., Xu, S., Yan, Y.: Cliff: Carrying location information in full frames into human pose and shape estimation. In: ECCV (2022) [4](#), [13](#)
30. Li, Z., Oskarsson, M., Heyden, A.: 3d human pose and shape estimation through collaborative learning and multi-view model-fitting. In: WACV (2021) [10](#)
31. Liang, J., Lin, M.C.: Shape-aware human pose and shape reconstruction using multi-view images. In: ICCV (2019) [3](#), [5](#), [9](#), [13](#)
32. Lin, J., Zeng, A., Wang, H., Zhang, L., Li, Y.: One-stage 3d whole-body mesh recovery with component aware transformer. In: CVPR (2023) [5](#)
33. Lin, K., Wang, L., Liu, Z.: End-to-end human pose and mesh reconstruction with transformers. In: CVPR (2021) [4](#), [13](#)
34. Lin, K., Wang, L., Liu, Z.: Mesh graphormer. In: ICCV (2021) [4](#)
35. Liu, Y., Wang, T., Zhang, X., Sun, J.: Petr: Position embedding transformation for multi-view 3d object detection. ECCV (2022) [3](#), [6](#), [7](#)
36. Loper, M., Mahmood, N., Black, M.J.: MoSh: Motion and shape capture from sparse markers. ACM TOG (2014) [9](#)
37. Loper, M., Mahmood, N., Romero, J., Pons-Moll, G., Black, M.J.: SMPL: A skinned multi-person linear model. ACM TOG (2015) [4](#), [5](#)
38. Ma, H., Chen, L., Kong, D., Wang, Z., Liu, X., Tang, H., Yan, X., Xie, Y., Lin, S.Y., Xie, X.: Transfusion: Cross-view fusion with transformer for 3d human pose estimation. In: BMVC (2021) [5](#)
39. Ma, X., Su, J., Wang, C., Zhu, W., Wang, Y.: 3d human mesh estimation from virtual markers. In: CVPR (2023) [4](#), [13](#)



40. von Marcard, T., Henschel, R., Black, M.J., Rosenhahn, B., Pons-Moll, G.: Recovering accurate 3d human pose in the wild using imus and a moving camera. In: ECCV (2018) 13
41. Mehta, D., Rhodin, H., Casas, D., Fua, P., Sotnychenko, O., Xu, W., Theobalt, C.: Monocular 3d human pose estimation in the wild using improved cnn supervision. In: 3DV (2017) 9
42. Moon, G., Lee, K.M.: I2l-meshnet: Image-to-lixel prediction network for accurate 3d human pose and mesh estimation from a single rgb image. In: ECCV (2020) 4, 13
43. Omran, M., Lassner, C., Pons-Moll, G., Gehler, P., Schiele, B.: Neural Body Fitting: Unifying deep learning and model-based human pose and shape estimation. In: 3DV (2018) 13
44. Pavlakos, G., Choutas, V., Ghorbani, N., Bolkart, T., Osman, A.A., Tzionas, D., Black, M.J.: Expressive body capture: 3D hands, face, and body from a single image. In: CVPR (2019) 4, 5
45. Pavlakos, G., Zhu, L., Zhou, X., Daniilidis, K.: Learning to estimate 3D human pose and shape from a single color image. In: CVPR (2018) 2, 4, 13
46. Shetty, K., Birkhold, A., Jaganathan, S., Strobel, N., Kowarschik, M., Maier, A., Egger, B.: PLIKs: A pseudo-linear inverse kinematic solver for 3D human body estimation. In: CVPR (2023) 13
47. Shin, S., Halilaj, E.: Multi-view human pose and shape estimation using learnable volumetric aggregation. arXiv preprint arXiv:2011.13427 (2020) 3, 5, 9, 13
48. Shuai, H., Wu, L., Liu, Q.: Adaptive multi-view and temporal fusing transformer for 3d human pose estimation. IEEE TPAMI (2022) 5
49. Sigal, L., Balan, A., Black, M.: Combined discriminative and generative articulated pose and non-rigid shape estimation. In: NeurIPS (2007) 4
50. Song, J., Chen, X., Hilliges, O.: Human body model fitting by learned gradient descent. In: ECCV (2020) 13
51. Tian, Y., Zhang, H., Liu, Y., Wang, L.: Recovering 3d human mesh from monocular images: A survey. IEEE TPAMI (2023) 5
52. Tiwari, G., Antic, D., Lenssen, J.E., Sarafianos, N., Tung, T., Pons-Moll, G.: Pose-ndf: Modeling human pose manifolds with neural distance fields. In: ECCV (2022) 4
53. Trumble, M., Gilbert, A., Malleon, C., Hilton, A., Collomosse, J.: Total capture: 3d human pose estimation fusing video and inertial sensors. In: BMVC (2017) 9, 13
54. Trumble, M., Gilbert, A., Hilton, A., Collomosse, J.: Deep autoencoder for combined human pose estimation and body model upscaling. In: ECCV (2018) 13
55. Vaswani, A., Shazeer, N., Parmar, N., Uszkoreit, J., Jones, L., Gomez, A.N., Kaiser, L., Polosukhin, I.: Attention is all you need. In: NeurIPS (2017) 4
56. Wei, S.E., Ramakrishna, V., Kanade, T., Sheikh, Y.: Convolutional pose machines. In: CVPR (2016) 13
57. Xiang, D., Joo, H., Sheikh, Y.: Monocular total capture: Posing face, body, and hands in the wild. In: CVPR (2019) 4
58. Xu, Y., Zhu, S.C., Tung, T.: DenseRaC: Joint 3D pose and shape estimation by dense render-and-compare. In: ICCV (2019) 13
59. Yang, S., Heng, W., Liu, G., Luo, G., Yang, W., Yu, G.: Capturing the motion of every joint: 3d human pose and shape estimation with independent tokens. In: ICLR (2023) 4
60. Yoshiyasu, Y.: Deformable mesh transformer for 3d human mesh recovery. In: CVPR (2023) 4

61. Yu, Z., Zhang, L., Xu, Y., Tang, C., Tran, L., Keskin, C., Park, H.S.: Multiview human body reconstruction from uncalibrated cameras. In: NeurIPS (2022) [3](#), [5](#), [11](#), [12](#), [13](#)
62. Zanfir, A., Marinoiu, E., Sminchisescu, C.: Monocular 3D pose and shape estimation of multiple people in natural scenes - the importance of multiple scene constraints. In: CVPR (2018) [4](#)
63. Zeng, W., Ouyang, W., Luo, P., Liu, W., Wang, X.: 3D human mesh regression with dense correspondence. In: CVPR (2020) [13](#)
64. Zhang, H., Cao, J., Lu, G., Ouyang, W., Sun, Z.: DaNet: Decompose-and-aggregate network for 3D human shape and pose estimation. In: ACM MM (2019) [13](#)
65. Zhang, H., Tian, Y., Zhang, Y., Li, M., An, L., Sun, Z., Liu, Y.: PyMAF-X: Towards well-aligned full-body model regression from monocular images. IEEE TPAMI (2023) [13](#)
66. Zhang, H., Tian, Y., Zhou, X., Ouyang, W., Liu, Y., Wang, L., Sun, Z.: PyMAF: 3D human pose and shape regression with pyramidal mesh alignment feedback loop. In: ICCV (2021) [4](#), [13](#)
67. Zhang, Z., Wang, C., Qin, W., Zeng, W.: Fusing wearable imus with multi-view images for human pose estimation: A geometric approach. In: CVPR (2020) [13](#)
68. Zheng, C., Liu, X., Qi, G.J., Chen, C.: POTTER: Pooling attention transformer for efficient human mesh recovery. In: CVPR (2023) [4](#), [13](#)
69. Zheng, C., Mendieta, M., Yang, T., Qi, G.J., Chen, C.: Feater: An efficient network for human reconstruction via feature map-based transformer. In: CVPR (2023) [4](#), [13](#)
70. Zhou, K., Zhang, L., Lu, F., Zhou, X.D., Shi, Y.: Efficient hierarchical multi-view fusion transformer for 3d human pose estimation. In: ACM MM (2023) [5](#)

## A Images from Unseen Views

Our method can recover human mesh from arbitrary multi-view images, including images from totally unseen camera views. For MPI-INF-3DHP and Total-Capture datasets, models are trained on 4 camera views by default as done in the main manuscript. As these two datasets provide more than 4 camera views, we test the model on totally unseen camera views of them, *i.e.*, we randomly select an arbitrary number of unseen camera views and recover human mesh from them. The results are shown in Figure 5. We can observe that our method performs well even on totally unseen camera views.

## B Arbitrary Multi-view Images

In this section, we show visualization results of human mesh recovery from arbitrary multi-view images. As described in the main manuscript, the term “arbitrary” involves two characteristics: the arbitrary angle and arbitrary number of views. Thus, for each of the three datasets (Human3.6M, MPI-INF-3DHP and TotalCapture), we randomly select an arbitrary number of all available (seen and unseen) camera views and recovery human mesh from them. The results are show in Figure 6 and Figure 7. The results demonstrate the flexibility of our method.



**Fig. 5: Visualization results of human mesh recovery from unseen camera views.** We show the results from different number (1-4) of totally unseen views on MPI-INF-3DHP and TotalCapture datasets. For each sample, we show the input image, the reconstruction overlay and the top view.

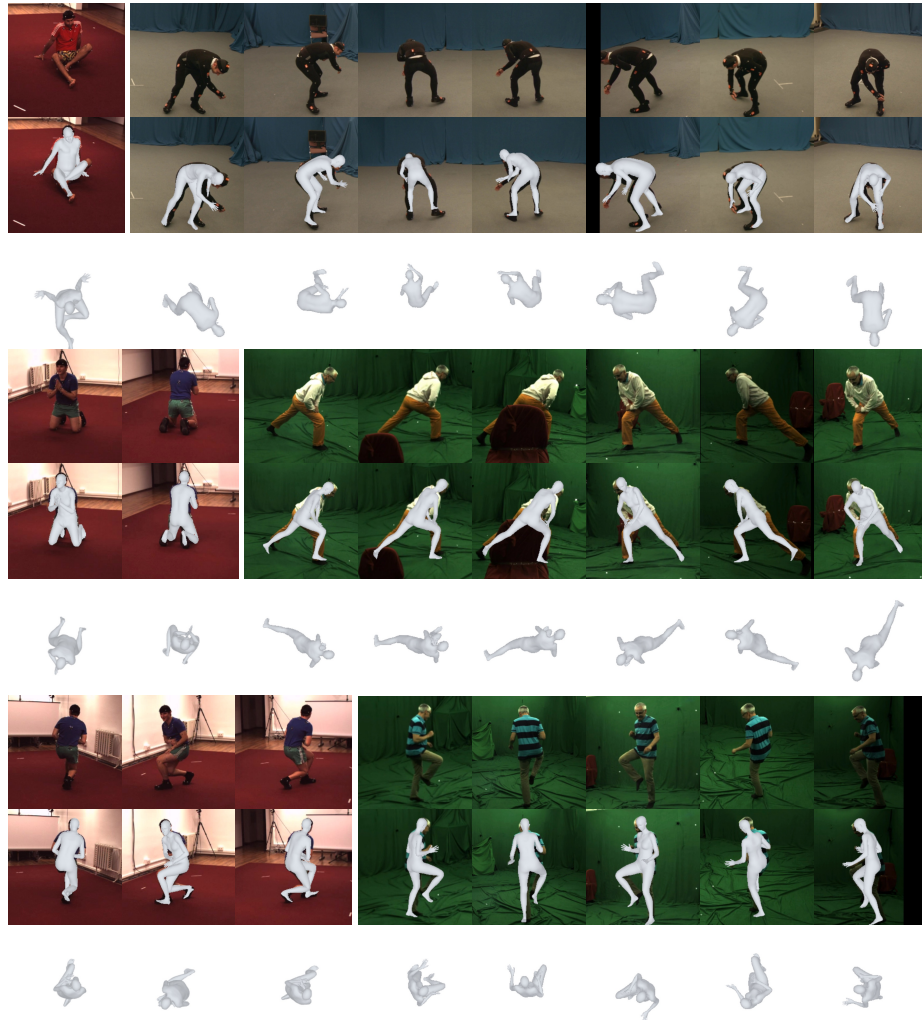


**Fig. 6: Visualization results of human mesh recovery from arbitrary multi-view images.** Results from 1-3 and 5-7 camera views on different datasets are shown. For each sample, we show the input image, the reconstruction overlay and the top view.

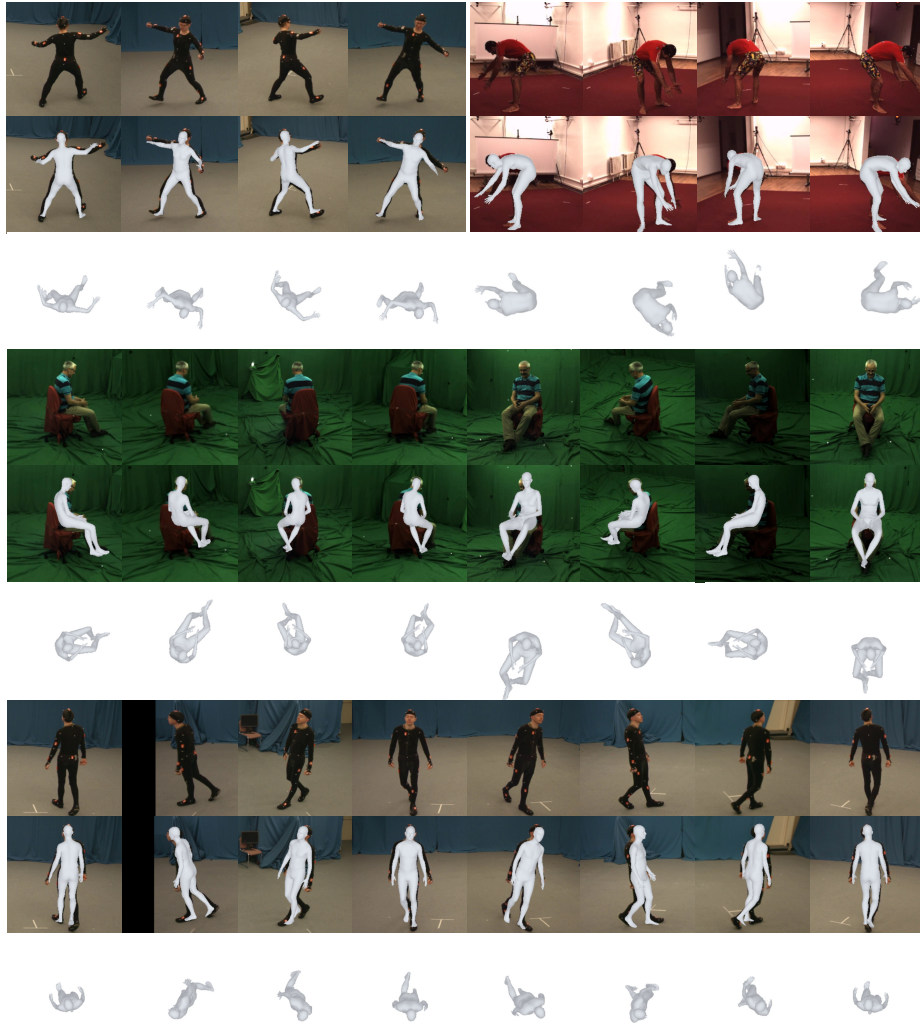


**Fig. 7: Visualization results of human mesh recovery from arbitrary multi-view images.** Results from 4 and 8 camera views on different datasets are shown. For each sample, we show the input image, the reconstruction overlay and the top view.